Flood Projection in Support of Dike Structure Improvements in New Brunswick, Canada

Hossein Amini [1], Shabnam Jabari [1]*, Heather McGrath [2], Mikhail Sokolov [2], Othman Nasir [1]

[1] Department of Geodesy & Geomatics Engineering, University of New Brunswick, Fredericton, NB E3B 5A3, Canada – hossein.amini1994@unb.ca – sh.jabari@unb.ca – onasir@unb.ca
[2] Natural Resources Canada, Ottawa, ON K1S 5K2, Canada – heather.mcgrath@ nrcan-rncan.gc.ca – mikhail.sokolov@nrcan-rncan.gc.ca

KEYWORDS: Flood Mapping, Super-Resolution, ESRGAN, Deep Learning, HAND model, Climate Change.

1. Introduction

Climate change-induced sea-level rise is predicted to exacerbate the catastrophic damage of floods in the future, especially in coastal areas (Didier et al. 2019). This effect is particularly challenging for Atlantic Canada as the water level is predicted to rise by around 1m on different shorelines of the region. The area is also known for high tidal effects, exacerbating the challenge. In our study area, in Memramcook, New Brunswick, Canada, there exists a historical dike structure along the river to protect the agricultural and urban lands from the high tidal effects of the Memramcook River. However, the rise in climate change-induced water levels is predicted to overflow the dike system, making it dangerous for the surrounding lands. In this project, we aimed to predict the effect of the water level rise in the area to elevate the dike structure.

One of the effective methods for predicting inundated areas is the Hight Above the Nearest Drainage (HAND) model (McGrath et al. 2018). HAND models can be created with digital terrain models (DTM) generated using different methods, including LiDAR data, which is the data used in this study.

In inundation prediction using a HAND model, a water level observation derived from gauge stations is utilized to threshold the HAND values to predict the water body polygons. However, in our study area, no gauge observations exist near the river. Thus, to extract the required thresholds, we obtained the water extent polygons from the satellite imagery of existing flood events.

The final goal of this project is to add the water level raised by climate change to the water level of the worst flood events in the area to predict the vulnerability of the surrounding lands in the worst-case scenario. With this elevated water level, the local government can plan to increase the elevation of the existing dike structure.

The flood events detected in the historical images of the study area date back to the 1970s when the only satellite observation available was through Landsat sensors with a 30-m spatial resolution (for the sake of brevity, in this study, we refer to spatial resolution as resolution). Therefore, to overcome the resolution gap, we employed a Super-Resolution technique on the archived satellite imagery to enhance the threshold selection process.

Super-resolution is regarded as an up-sampling technique as an alternative to more traditional methods like cubic resampling and pan-sharpening (Lezine et al. 2021, Vivone et al. 2015). There have been successful attempts to use Generative Adversarial Networks (GANs) in Super-Resolution so far (Rabbi et al. 2020). These networks consist of two Convolutional Neural Networks (CNNs), including a generator responsible for generating outputs with similar statistics as input data and a discriminator that is responsible for evaluating the likelihood of the outputs originating from the training dataset. With the training dataset including pairs of Low-Resolution (LR) and High-Resolution (HR) images, the generator upscales the LR images to the resolution of HR images to produce SR images. This step is then followed by the discriminator evaluating the accuracy of the generated SR image. In the study carried out by Lezine et al. (2021), the authors trained the ESRGAN model using three bands (NIR/Green/Red) of pairs of HR and artificially coarsened LR satellite images in an attempt to test a potential improvement on surface water classification, reaching improved results, especially at higher resampling factors. Although well-established and applicable in many areas, to the best of our knowledge, SR-GANs have not been extensively investigated in flood mapping applications. This study attempted to investigate the application of ESRGAN to detect the water body threshold for the HAND model in our study area.

1. Methodology

In this study, we employed Enhanced Super-Resolution Generative Adversarial Networks (ESRGAN) developed by Wang et al. (2018) to assess a potential improvement in water body classification. Then, we used the classified waterbody to find HAND model threshold. Finally, the water level rise due to climate change is added to the threshold to find the future waterbody polygon. The flowchart of this project is presented in Figure 1.

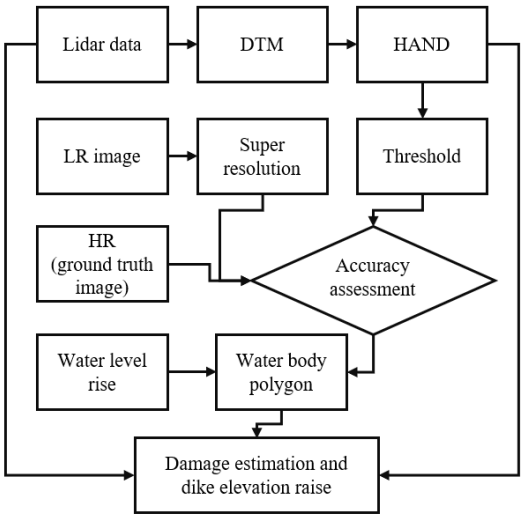

Figure 1. Flowchart of the proposed work

* Corresponding (presenting) author

In this study, we obtained an LR image from a flood event and a matching HR ground truth image with similar conditions in terms of tidal effects and water level. This approach was necessary to ensure a high level of consistency in the analysis, acknowledging the fact that the time of data acquisition for these images was not the same. Table 2 shows the specifications of the data used in this study.

Dataset	Resolution	Data time (UTC)	Info
Landsat-8 image	30 m	Aug 2, 2016, 15:01	LR image
WorldView-3 image	0.5 m	Oct 15, 2016, 15:38	HR image (ground truth)
LiDAR point clouds	6 points/m^2	Aug 2 – Sep 28, 2015	LiDAR data for DTM

Table 1. Information about the datasets used in this study

We used the ESRGAN trained on satellite imagery by Lezine et al. (2021) to generate SR images. By applying resampling factors of 4X and 10X, we generated SR images with 7.5m and 3m resolutions, respectively. Subsequently, using the Normalized Water Difference Index (NDWI), water classification was performed on LR, HR, and SR images. NDWI is calculated from the Green and Near-Infrared (NIR) bands using Equation (1).

NDWI = (Green - NIR) / (Green + NIR) (1)

2. Results and Accuracy Assessment

To conduct a comparative accuracy assessment without biasing the results by an extensive number of water pixels, the resulting water bodies were masked to a buffer zone of 60 meters around the river body to better compare the classified water/non-water pixels in the images. The formula for the accuracy assessment, calculated from parameters such as True Positive (TP), True Negative (TN), False Positive (FP), False Negative (FN), relative observed agreement among raters (p0), and hypothetical probability of chance agreement (pe), are shown in Table 2.

Accuracy Metric	Formula
Overall Accuracy	$\frac{TP + TN}{TP + TN + FP + FN}$
Precision	$\frac{TP}{TP + FP}$
Recall	$\frac{TP}{TP + FN}$
F1 Score	$\frac{Precision\,.Recall}{Precision + Recall}$
Kappa Coefficient	$\frac{p0 - pe}{1 - pe}$

Table 2. Formula used for accuracy assessment

The results of the accuracy assessment, shown in Table 3, revealed an improvement in water classification in the 7.5m resolution SR (4X) image over the original LR image, as well as in the 3m resolution SR (10X) image over the 7.5m resolution SR image. Both 4X and 10X SR images showed higher overall accuracy compared to the LR image. Accounting for change agreement, the Kappa coefficient for the SR images also revealed a robust improvement over the LR image. The recall for the 10X SR image demonstrates a noticeable improvement in identifying all instances of water compared to the LR image, which is crucial in flood mapping applications. On the other hand, precision for the LR image was slightly higher, while a higher F1 score in SR images indicated a better balance between the precision and the sensitivity of the classification.

The next step in accuracy assessment is to compare the results of the thresholded HAND model to an existing flood satellite image, which will be presented in the full paper.

	Resolution (m)	Image	Overall Accuracy	Kappa	Recall	Precision	F1 Score
1X	3	LR (original)	0.92	0.74	0.83	0.99	0.91
4X	7.5	LR (resampled)	0.88	0.75	0.78	0.93	0.85
		SR	0.89	0.77	0.80	0.93	0.86
10X	3	LR (resampled)	0.88	0.76	0.76	0.94	0.85
		SR	0.89	0.77	0.82	0.92	0.86

Table 3. Results of accuracy assessment for different sharpening factors.

3. References

Messner, F., & Meyer, V. (2006). Flood damage, vulnerability and risk perception–challenges for flood damage research. In Flood risk management: hazards, vulnerability and mitigation measures (pp. 149-167). Dordrecht: Springer Netherlands.

Thistlethwaite, J., Henstra, D., Brown, C., & Scott, D. (2018). How flood experience and risk perception influences protective actions and behaviours among Canadian homeowners. Environmental management, 61(2), 197-208.

Didier, D., Bandet, M., Bernatchez, P., & Dumont, D. (2019). Modelling coastal flood propagation under sea level rise: a case study in Maria, Eastern Canada. Geosciences, 9(2), 76.

McGrath, H., Bourgon, J. F., Proulx-Bourque, J. S., Nastev, M., & Abo El Ezz, A. (2018). A comparison of simplified conceptual models for rapid web-based flood inundation mapping. Natural Hazards, 93, 905-920.

Wang, X., Yu, K., Wu, S., Gu, J., Liu, Y., Dong, C., ... & Change Loy, C. (2018). Esrgan: Enhanced super-resolution generative adversarial networks. In Proceedings of the European conference on computer vision (ECCV) workshops (pp. 0-0).

Lezine, E. M., Kyzivat, E. D., & Smith, L. C. (2021). Super-Resolution Surface Water Mapping on the Canadian Shield Using Planet CubeSat Images and a Generative Adversarial Network. Canadian Journal of Remote Sensing, 47(2), 261-275.

Vivone, G., Alparone, L., Chanussot, J., Dalla Mura, M., Garzelli, A., Licciardi, G. A., ... & Wald, L. (2014). A critical comparison among pansharpening algorithms. IEEE Transactions on Geoscience and Remote Sensing, 53(5), 2565-2586.

Rabbi, J., Ray, N., Schubert, M., Chowdhury, S., & Chao, D. (2020). Small-object detection in remote sensing images with end-to-end edge-enhanced GAN and object detector network. Remote Sensing, 12(9), 1432.